Journal Pre-proofs

Research papers

Divergent sensitivity of surface water and energy variables to precipitation product uncertainty in the Tibetan Plateau

Wei Qi, Junguo Liu, Jun Xia, Deliang Chen

PII: S0022-1694(19)31073-X
DOI: https://doi.org/10.1016/j.jhydrol.2019.124338
Reference: HYDROL 124338

To appear in: *Journal of Hydrology*

Received Date: 4 June 2019
Revised Date: 6 November 2019
Accepted Date: 7 November 2019

Please cite this article as: Qi, W., Liu, J., Xia, J., Chen, D., Divergent sensitivity of surface water and energy variables to precipitation product uncertainty in the Tibetan Plateau, *Journal of Hydrology* (2019), doi: https://doi.org/10.1016/j.jhydrol.2019.124338

Divergent sensitivity of surface water and energy variables to precipitation product uncertainty in the Tibetan Plateau

Wei Qi [a], Junguo Liu [a *], Jun Xia [b], Deliang Chen [c]

[a] School of Environmental Science and Engineering, Southern University of Science and Technology, Shenzhen, 518055, China

[b] State Key Laboratory of Water Resources & Hydropower Engineering Science, Wuhan University, Wuhan, 430072, China

[c] Regional Climate Group, Department of Earth Sciences, University of Gothenburg, Gothenburg, Box 460 S-405 30, Sweden

[*]Email: junguo.liu@gmail.com; liujg@sustech.edu.cn

Abstract:

Precipitation is a major driving factor for land surface water and energy balances. Uncertainty in global precipitation products over observation sparse regions such as the Tibetan Plateau (TP) is generally large. Sensitivity of surface water and energy variables to precipitation uncertainty can provide clues for confidence that can be assigned to simulated water and energy variables in such regions. In this study, the sensitivities of surface water and energy variables to global precipitation product uncertainty over four large river basins in the TP are quantified and inter-compared based on a newly developed sensitivity analysis approach. A water and energy budget-based distributed hydrological model including biosphere is utilized after calibration and validation against observed runoff and Land Surface Temperatures (LSTs) from Moderate Resolution Imaging Spectroradiometer (MODIS). Eight global precipitation products are used to represent the precipitation uncertainty. Results show that Canopy interception loss (CIE) and runoff are highly sensitive to the uncertainty in general, whereas LSTs are not sensitive. Therefore, confidence in simulated CIE and runoff can be considered relatively low when using global precipitation products in the four basins. These results imply that other simulated variables may have large uncertainty even when LSTs simulation performs well, and accurate simulations of CIE and runoff require high accuracy in precipitation. Because CIE has profound influence on local hydrological cycle, the results also imply that utilizing the most accurate precipitation product is critical for local scale hydrological cycle research.

Key words: Precipitation Uncertainty; Runoff; Sensitivity; Tibetan Plateau; Water Balance; Distributed hydrological modeling

1 Introduction

The Tibetan Plateau (TP) plays an important role in ensuring regional water security, food security and sustainable socioeconomic development in South, East and Southeast Asia. The majority of in situ precipitation stations are located in the southern and eastern TP (Gao and Liu, 2013; Yang et al., 2014). To compensate the data gap in the data sparse regions in the TP, satellite- and/or reanalysis-based global precipitation products are utilized as input of land surface/hydrological models to simulate water and energy variables (e.g., Xue et al. (2013)).

Precipitation has large temporal and spatial variations which render reliable estimation difficult (Ji and Kang, 2015). In addition, because global satellite- and/or reanalysis-based precipitation products use different inversion algorithms and data sources with limited in situ gauge observation, global precipitation products have various pros and cons. For example, Qi et al. (2016a) showed that Tropical Rainfall Measuring Mission (TRMM) products - TRMM3B42 (Huffman et al., 2007) and Global Land Data Assimilation System (GLDAS) version 1 (Rodell et al., 2004) underestimate heavy rainfall intensities in summer periods on a daily scale in a coastal river basin; Chen et al. (2018) found that satellite products are generally more realistic than those from reanalysises. Because of the uncertainty of precipitation products, confidence in simulated land surface water and energy variables using them is unknown (Biemans et al., 2009; Wang et al., 2011; Zhou et al., 2013; Qi et al., 2016a; Qi et al., 2018b), which to some extent has undermined the practical applications of global precipitation products for water and energy variable simulations in data sparse region in the TP.

Sensitivity analysis of water and energy variables to precipitation uncertainties can provide information on which variable is influenced the most and which one is least impacted.

Therefore, the sensitivity can provide information on confidence that we can place on simulated various water and energy variables when using global precipitation products in data sparse regions. Fekete et al. (2004) investigated the influence of precipitation uncertainty on runoff on a global scale; Guo et al. (2006) studied the sensitivity of soil moisture to meteorological forcing in Russian, United States, China and Mongolia; Kato et al. (2007) first employed an ensemble including different land surface models and precipitation products to simulate water and energy fluxes in the United States; Wei et al. (2008) investigated the sensitivity of soil moisture to precipitation and radiation; Wang and Zeng (2011) studied the sensitivity of soil moisture, evapotranspiration and simulated runoff to precipitation and air temperature uncertainties. However, these studies did not verify their simulation accuracy against observation, which could undermine the results because the simulations may have large uncertainties if simulation is not validated.

Many studies also investigated sensitivity of simulation results to precipitation uncertainties using calibrated models. For example, Biemans et al. (2009), Vano et al. (2012) and Weiland et al. (2015) studied influence of precipitation uncertainty on runoff using calibrated hydrological models; Kavetski et al. (2006b) and Kavetski et al. (2006a) developed a mathematical approach and studied the influence of precipitation uncertainty on runoff simulation. Although the previous studies used calibrated models, the sensitivity analysis were carried out only for runoff, and therefore the sensitivity of different water and energy variables cannot be inter-compared. Thus, more comprehensive studies on water and energy variable sensitivity to global precipitation product uncertainties are needed based on well calibrated and validated hydrological/land surface models.

The overall aim of this study is to investigate the sensitivity of land surface water and energy variables to global precipitation product uncertainty in the TP. A water and energy budget-based distributed hydrological model including biosphere (WEB-DHM) (Wang et al., 2009a; Wang et al., 2009b; Wang et al., 2009c; Qi et al., 2015) is implemented after calibration and validation based on hydrological gauge observation and Moderate Resolution Imaging Spectroradiometer (MODIS) Land Surface Temperature (LST) (the MOD11A2 product) (Wan, 2008). Eight global scale fine resolution precipitation products are utilized to represent the precipitation uncertainty. This paper is unique in that, for the first time, divergent sensitivity of various water and energy variables to global precipitation product uncertainty is quantified and inter-compared in the TP. The results can provide important information on different confidence that can be placed on various simulated water and energy variables when using global precipitation products in the data sparse regions in the TP.

2 Study basins, model, data and assessment criteria

2.1 River basins studied

Four large river basins (Fig. 1) in the TP were used to conduct this study. They cover a total area of 571,471 km^2. The average elevations of the river basins are above 4100 meters. The mean annual temperatures in the four river basins are around zero degree celsius. Among the four river basins, the Yarlung Tsangpo River basin is the largest (256,864 km^2), and the Upper Lancang River basin is the smallest (53,656 km^2). The Upper Yangtze River basin has an area of 137,371 km^2, and the Upper Yellow River basin has an area of 123,580 km^2. The river basin details are shown in Table 1 including basin average Leaf Area Index (LAI), aridity index, climate and hydrological regimes. Because this study is a sequel to our previous study, more river basin details can be found in the study by Qi et al. (2018a).

< Figure 1 here please >

< Table 1 here please >

2.2 Model and datasets

WEB-DHM combines a simple biosphere scheme version 2 (SiB2) land surface model (Sellers et al., 1986; Sellers et al., 1996a; Sellers et al., 1996b) and a hydrological model developed by Yang (1998). WEB-DHM simulates the leaf photosynthetic activity by combining a leaf stomatal conductance model developed by Ball (1988) and a photosynthesis model developed by Collatz et al. (1991) and Collatz et al. (1992) (i.e., the Ball-Berry model). WEB-DHM estimates LST from canopy temperature ($\mathrm{LST_c}$) and surface soil temperature ($\mathrm{LST_g}$) as below (Wang et al., 2009c)

$$LST_{sim} = \left[V \times LST_c^4 + (1 - V) \times LST_g^4 \right]^{1/4} \tag{2}$$

$$V = LAI / LAI_{max} \tag{3}$$

where V represents green vegetation coverage; LAI_{max} represents the maximum LAI defined by Sellers et al. (1996b). Many evaluations and applications using WEB-DHM have been conducted (Wang et al., 2010a; Wang et al., 2010b; Wang et al., 2012; Qi et al., 2015; Qi et al., 2016a; Qi et al., 2019), and results showed that WEB-DHM performs well generally.

China Gauge-based Daily Precipitation Analysis data is utilized in the model calibration and validation, and the precipitation data has been used in many studies showing good performance in general (Zhao and Zhu, 2015; Shen and Xiong, 2016; Gao et al., 2017). Hourly precipitation data are downscaled from the daily data using a stochastic method (Wang et al., 2011). Other model forcing data used are from the China Meteorological Forcing Dataset (CMFD) (He and Yang, 2011; Xue et al., 2013; Zhou et al., 2015; Yang et al., 2017). CMFD has a 3-hour temporal resolution. In the CMFD dataset, temperature, pressure, humidity and wind speed are instantaneous variables, and downward shortwave and longwave radiation are 3-hour mean values. Linear interpolation approaches are used to generate hourly data for temperature, pressure, humidity and wind speed. Downward shortwave and longwave radiation are assumed the same within each 3-hour time step. The 8-day MODIS land surface temperatures used (i.e. the MOD11A2 product) were observed at the day around 11:00 and at night around 22:00 (local time). Details about the model calibration and validation methods can be found in the study by Qi et al. (2018a). The global precipitation products used are listed in Table 2. The precipitation products used here are the same to our previous study (Qi et al., 2018a), and please refer to the previous study for more detailed description about the global precipitation products.

< Table 2 here please >

2.3 Assessment criteria

The sensitivity is quantified based on the Precipitation Uncertainty Influence (PUI) index using Eq. (4)

$$\mathrm{PUI} = \sum_{i=1}^{12} \left\{ \max\left(I_i\right) - \min\left(I_i\right) \right\} \Big/ \left[12 \cdot \mathrm{mean}\left\{ \mathrm{abs}\left(D_{obs}\right) \right\} \right] \tag{4}$$

where $\max\left(I_i\right)$ and $\min\left(I_i\right)$ represent the maximum and minimum values of simulated ensemble intervals in i*th* month; D_{obs} represents observation or simulated values utilizing observation. PUI index represents the average width of ensemble intervals normalized using D_{obs}. The higher the PUI, the wider the ensemble intervals on average (more sensitive). It can be seen that the PUI sensitivity index is different from previous methods, such as the one-factor-at-a-time sensitivity analysis method and Sobol''s sensitivity analysis approach, which are designed to quantify sensitivity of model outputs to various influential factors and do not consider ensemble interval width (Sobol, 2001; Tang et al., 2007a; Tang et al., 2007b; Fu et al., 2012; Zhang et al., 2013a). Nevertheless, the PUI sensitivity index considers ensemble interval width, which is appropriate because an ensemble of precipitation product data is utilized.

Coefficient of determination (R^2), mean bias error (MBE) and root mean square error (RMSE) are used in uncertainty assessment:

$$\mathrm{MBE} = \frac{\left(\sum_{i=1}^{n} X_{si} - \sum_{i=1}^{n} X_{oi}\right)}{n} \tag{5}$$

$$\mathrm{RMSE} = \sqrt{\frac{\sum_{i=1}^{n}\left(X_{si} - X_{oi}\right)^2}{n}} \tag{6}$$

where X_{oi} and X_{si} represent observation or simulation using observation and simulation forced by global precipitation products at time i. For runoff, Nash-Sutcliffe Efficiency (NSE) and relative bias (RB) are utilized (Qi et al., 2016b; Qi et al., 2016c; Qi et al., 2018c). NSE and RB are calculated as follows:

$$\mathrm{NSE} = 1 - \frac{\sum_{i=1}^{n}\left(Q_{pi} - Q_{ti}\right)^2}{\sum_{i=1}^{n}\left(Q_{ti} - \overline{Q_t}\right)^2} \tag{7}$$

$$\mathrm{RB} = \frac{\sum_{i=1}^{n} Q_{pi} - \sum_{i=1}^{n} Q_{ti}}{\sum_{i=1}^{n} Q_{ti}} \times 100\% \tag{8}$$

where Q_{pi} and Q_{ti} represent simulated and observed runoff; $\overline{Q_t}$ represents average runoff observation.

3 Results and discussion

3.1 Model validation

WEB-DHM has been calibrated and validated using observed runoff from 2000 to 2010 in the four river basins in our previous study (please refer to Fig. 2, Fig. 3, Table 3 and Table 4 of Qi et al. (2018a)). WEB-DHM shows good performance in replicating runoff observations with NSE being above 0.88 and absolute values of RB being lower than 9%. MODIS LSTs and WEB-DHM simulation are compared in Fig. 2. WEB-DHM simulated LSTs replicate MODIS observation well at both nightime and daytime. In the four river basins, the R^2 values all are higher than 0.83; RMSE values are lower than 4.36; absolute values of MBE are lower than 0.41. The uncertainty may be due to the input data of the model simulation. The linear green vegetation coverage (Eq. (2)) may also contribute the uncertainty of LST simulation. Overall, the performance of WEB-DHM is acceptable in reproducing the observed runoff and LSTs in the four river basins. The runoff and LSTs represent water and energy states, respectively. They are readily available from hydrological gauges and remote sensing products with good credibility, and therefore have been commonly used to validate model performance in simulating land surface water and energy processes (e.g., Wang et al. (2009c), Wang et al. (2011), Zhou et al. (2015), Wang et al. (2016)). This study follows the same approach to verify the model simulation.

< Figure 2 here please >

3.2 Simulated water and energy variables

Fig. 3 shows the ensemble of long term mean monthly simulation results in the Yarlong Tsangpo River basin. The results include sensible heat flux, latent heat flux, evapotranspiration (ET), Canopy interception loss (CIE), surface soil evaporation, ground interception store evaporation (GIE), surface zone wetness, land surface temperature (LST), upward shortwave radiation, upward longwave radiation, net radiation, ground heat flux and runoff.

< Figure 3 here please >

The ensemble of sensible heat flux (Fig. 3a) brackets observation-based results in most of the months except in May. Similarly, the ensemble of ground interception store evaporation (Fig. 3g) also does not bracket observation-based results in several months. However, the upper bounds of the ensembles of sensible heat flux and ground interception store evaporation are very close to observation-based simulation results. Different from sensible heat flux and ground interception store evaporation, the generated ensembles of other variables envelop the simulated results forced by observed precipitation. Regarding the spread of the ensembles, LST, upward shortwave radiation, upward longwave radiation, net radiation and ground heat flux show very narrow ensemble intervals, and are very similar to the observation /observation-based results. For other variables, the simulation ensembles show large intervals. This indicates that LST, upward shortwave radiation, upward longwave radiation, net radiation and ground heat flux are less sensitivity to precipitation uncertainties than other variables. The difference also implies that the simulations of the other variables may not be accurate even when LST, upward shortwave radiation, upward longwave radiation, net radiation and ground heat flux simulations are close to observation. Most of the results show the runoff is overestimated, which is because most of the precipitation products have higher precipitation estimation than observation (as shown in the Fig. 11 of Qi et al. (2018a)).

Fig. 4 shows comparison between ensemble averages and observation/observation-based simulation results in the Yarlong Tsangpo River basin. The ensemble averages reflect the seasonal variations of all variables well with R^2 values being over 0.97 overall. Large differences between ensemble averages and observation/observation-based simulation also exist. For example, the ensemble averages of ground interception store evaporation (Fig. 4g) are higher than observation-based simulation from January to March, and greatly lower from May to September; the ensemble averages of runoff are greatly higher than observation from June to September. The higher values of the ensemble average of runoff may be because the ensemble average of ET is close to simulation forced by observation (Fig. 4c), and ensemble average of precipitation is higher than observation (RB is up to 35%).

< Figure 4 here please >

Figs. 5, 6 and 7 show long term mean monthly simulation results in the Upper Lancang, Upper Yangtze and Upper Yellow River basins. The patterns are similar to the Yarlong Tsangpo River basin (Fig. 3): the various precipitation products result in different simulation results and the ensemble spreads of LST, upward shortwave radiation, upward longwave radiation, net radiation and ground heat flux are generally smaller than other variables. Figs. 8, 9 and 10 show comparison between ensemble averages and observation/observation-based simulation results. Similar to Fig. 4, the ensemble averages replicate the seasonal variations of all variables well, and the differences between ensemble averages and observation/observation-based simulation results vary with the variables.

< Figure 5 here please >

< Figure 6 here please >

< Figure 7 here please >

< Figure 8 here please >

< Figure 9 here please >

< Figure 10 here please >

3.3 Quantification of sensitivity

Fig. 11 shows the PUI index values of water and energy variables. The higher the PUI index values, the greater the influence of precipitation uncertainty. In the Yarlung Tsangpo River, PUI of runoff is the highest, and PUI of CIE is the second highest. Meanwhile, PUI value of LST is the lowest. Similarly, runoff is the most sensitive variable and LST is the least sensitive variable in the Upper Yellow and Upper Lancang Rivers. Nevertheless, in the Upper Yangtze River, GIE is the most sensitive variable, and LST is the least sensitive variable. The difference between the Upper Yangtze River and other three river basins may be because the Upper Yangtze River is dryer than others and also have relatively lower average LAI (as shown in Table 1). Overall, runoff is more sensitive than most of the other variables. In the river basins studied, the correlation between precipitation and runoff is high (Zhang et al., 2013b; Chen et al., 2017; Liu et al., 2018; Han et al., 2019). Therefore, the uncertainty in the precipitation has a large influence on runoff.

< Figure 11 here please >

The results in Fig. 11 indicate that CIE is the second most sensitive variable to precipitation uncertainty in the Yarlung Tsangpo and the Upper Lancang Rivers, and CIE is the third most sensitive variable in the Upper Yellow and the Upper Yangtze Rivers. Nevertheless, the PUI index values of CT and CIE are very similar in the Upper Yellow River. The average LAI in the Upper Yellow River is the highest among the four river basins, which may result in that the ranking of CT is higher than other three river basins. In the Upper Yangtze River basin, the average LAI is low comparatively. Meanwhile, the Upper Yangtze River basin is the driest among the four river basins. Therefore, GIE is more sensitive than CIE in the Upper Yangtze River basin. Overall, CIE is sensitive to precipitation uncertainty in the four river basins. As pointed out by Wang-Erlandsson et al. (2014) and van der Ent et al. (2014), CIE has profound influence on local hydrological cycle. Thus, utilizing the most accurate precipitation data is critical for studying local hydrological cycle in the TP.

The results in Fig. 11 provide information on the confidence that we can place on various simulated water and energy variables when utilizing global precipitation product data. Based on the results, when precipitation product data have uncertainty, the confidence should be decreasing from runoff/GIE to LST: least confidence should be given to the simulations of runoff/GIE and highest confidence to LST simulation. In addition to the information on the confidence, the results in Fig. 11 also have many implications. For example, a few studies suggested utilizing LSTs to calibrate the parameters of land surface/hydrological models (Corbari and Mancini, 2014; Silvestro et al., 2015; Koch et al., 2016). However, the results in Fig. 11 indicate that other simulated water and energy variables may have large uncertainties even when simulated LSTs perform well. When reliable hydrological gauge runoff data are not available, using Surface Zone Wetness (SW) (which could be obtained from satellite-based remote sensing data) to calibrate models may generate better results than using LSTs because SW is more sensitive than LSTs to precipitation uncertainty. In addition, the results in Fig. 11 also imply that the requirement on the accuracy of precipitation data may not be strict in LST simulation in data sparse regions because LSTs are least sensitive to precipitation uncertainty.

3.4 Discussion

The PUI index values are calculated on the basis of eleven years (from 2000 to 2010) of data on the annual scale in this study, and therefore the results in Fig. 11 are appropriate for long term mean annual scale studies which are common in large scale research and land surface and atmosphere interaction research (e.g., Wei et al. (2008); Wang-Erlandsson et al. (2014); Schellekens et al. (2017)). It should be noted that precipitation influence may change when study regions, precipitation data used, or/and hydrological/land surface models used vary. However, the developed sensitivity assessment criterion (i.e. Eq. (4)) is not case specific, and should be applicable to other studies. The results here do add important insights into the currently limited pool of knowledge regarding the distinguishing sensitivities of water and energy variables to uncertainties in precipitation data in the TP. As shown in Table 1, the average LAI of the four river basins range from 0.22 to 0.55, which brackets the average LAI value of the entire TP (0.29). In addition, the selected four river basins span several climate zones and different hydrological regimes (semiarid, dry sub-humid, humid, water-limited and energy-limited). Therefore, the results in this study should be applicable to other regions in the TP.

The results in Section 3.2 indicate some ensemble averages have good performance, which could also provide a reference for the confidence that could be put on simulated ensemble averages in data sparse regions. However, the confidence gained from the ensemble averages could be very similar for different variables because the ensemble averages of several variables have similar performance. Different from the confidence obtained from the ensemble averages, the sensitivity information in Fig. 11 distinguishes the difference in the confidence that could be assigned to each of the simulated variables. The WEB-DHM model has been calibrated and validated against the hydrological gauge observation and MODIS LSTs, and the results show WEB-DHM performs well (recall the results in Section 3.1). Thus, the input data processing, model calibration and validation approaches and calibrated parameters are considered appropriate and acceptable.

4 Conclusions

This study investigates the divergent sensitivity of various water and energy variables to precipitation uncertainty in the TP. Four large river basins with diversified vegetation coverages, climates and hydrological regimes are used. Eight global precipitation products are utilized as the input to a well calibrated and validated distributed hydrological model simulating water and energy budgets. This study is unique in that it quantified the distinguishing sensitivity of water and energy variables to precipitation uncertainty in the TP based on the newly developed sensitivity analysis approach. The results provide improved understanding and appropriate interpretation of water and energy variable simulations in the TP, when different global precipitation products are used to force the model. This knowledge is especially useful in data sparse regions like the TP. The major contributions of this study are summarized as follows.

First, runoff is more sensitive to precipitation uncertainties than most variables in general. Therefore, less confidence should be given to runoff simulation than others when using global precipitation products in ungauged regions.

Second, LSTs are least sensitive to precipitation uncertainty among all variables considered. More confidence can be attached to the simulated LSTs, and other variables may have large uncertainty even when simulated LSTs are accurate. This result implies that calibrating the parameters of land surface/hydrological models using LSTs could be problematic when precipitation has uncertainty.

Third, Canopy interception loss has a relatively high sensitivity to precipitation uncertainty. Because Canopy interception loss has profound influence on local hydrological cycle, utilizing the most accurate precipitation data is critical for realistically representing local scale hydrological cycle in the four basins on the TP.

The methodology introduced in this paper could be used in other regions. With more information on the sensitivity, more precise confidence information on simulated variables using global precipitation products could be gained in data sparse regions.

Acknowledgements:

This study was supported by the Strategic Priority Research Program of Chinese Academy of Sciences (XDA20060402), the Young Scientists Fund of the National Natural Science Foundation of China (51809136), and China Postdoctoral Science Foundation (2017M622516). Additional support was provided by Guangdong Provincial Key Laboratory of Soil and Groundwater Pollution Control (2017B030301012), and State Environmental Protection Key Laboratory of Integrated Surface Water-Groundwater Pollution Control. MODIS data were downloaded from USGS land processes distributed active archive center (https://lpdaac.usgs.gov/products/modis_products_table/mod15a2). GLDAS2.0 and GLDAS2.1 data were downloaded from https://hydro1.gesdisc.eosdis.nasa.gov/data/GLDAS/. CMORPH-BLD V1.0 was downloaded from ftp://ftp.cpc.ncep.noaa.gov/precip/CMORPH_V1.0/. PERSIANN-CDR was downloaded from https://www.ncei.noaa.gov/data/. TRMM3B42 was downloaded from http://mirador.gsfc.nasa.gov/cgi-bin/mirador/. WFDEI-CRU was downloaded from ftp.iiasa.ac.at. MSWEP V2.01 was downloaded from https://data.princetonclimate.com/opendap. CHIRPS V2.0 was downloaded from ftp://ftp.chg.ucsb.edu/. The observed discharge data used in this study were collected from hydrology bureaus. The authors are deeply indebted to editors and anonymous reviewers for their valuable time and constructive suggestions that greatly improved the quality of this paper.

References:

Ashouri H., Hsu K.-L., Sorooshian S., Braithwaite D.K., Knapp K.R., Cecil D.L., Nelson B.R., Prat O.P., 2015. PERSIANN-CDR: Daily Precipitation Climate Data Record from Multisatellite Observations for Hydrological and Climate Studies. Bulletin of the American Meteorological Society, 96(1): 69-83.

Ball J.T., 1988. An analysis of stomatal conductance, Stanford University, 89 pp.

Beck H.E., van Dijk A., Levizzani V., Schellekens J., Miralles D.G., Martens B., de Roo A., 2017. MSWEP: 3-hourly 0.25° global gridded precipitation (1979–2015) by merging gauge, satellite, and reanalysis data. Hydrology and Earth System Sciences, 21(1): 589-615.

Biemans H., Hutjes R.W.A., Kabat P., Strengers B.J., Gerten D., Rost S., 2009. Effects of Precipitation Uncertainty on Discharge Calculations for Main River Basins. Journal of Hydrometeorology, 10(4): 1011-1025.

Chen A., Chen D., Azorin‐Molina C., 2018. Assessing reliability of precipitation data over the Mekong River Basin: A comparison of ground‐based, satellite, and reanalysis datasets. International Journal of Climatology, 38(11): 4314-4334.

Chen X., Long D., Hong Y., Zeng C., Yan D., 2017. Improved modeling of snow and glacier melting by a progressive two - stage calibration strategy with GRACE and multisource data: How snow and glacier meltwater contributes to the runoff of the Upper Brahmaputra River basin? Water Resources Research, 53(3): 2431-2466.

Collatz G.J., Ribas-Carbo M., Berry J.A., 1992. Coupled Photosynthesis-Stomatal Conductance Model for Leaves of C4 Plants. Functional Plant Biology, 19(5): 519-538.

Collatz J.G., Ball T.J., Grivet C., Berry J.A., 1991. Physiological and environmental regulation of stomatal conductance, photosynthesis and transpiration: a model that includes a laminar boundary layer. Agricultural and Forest Meteorology: 107-136.

Corbari C., Mancini M., 2014. Calibration and Validation of a Distributed Energy–Water Balance Model Using Satellite Data of Land Surface Temperature and Ground Discharge Measurements. Journal of Hydrometeorology, 15(1): 376-392.

Fekete B.M., Vörösmarty C.J., Roads J.O., Willmott C.J., 2004. Uncertainties in Precipitation and Their Impacts on Runoff Estimates. Journal of Climate, 17(2): 294-304.

Fu G., Kapelan Z., Reed P., 2012. Reducing the Complexity of Multiobjective Water Distribution System Optimization through Global Sensitivity Analysis. Journal of Water Resources Planning and Management, 138(3): 196-207.

Funk C. et al., 2015a. The climate hazards infrared precipitation with stations—a new environmental record for monitoring extremes. Scientific Data, 2.

Funk C., Verdin A., Michaelsen J., Peterson P., Pedreros D., Husak G., 2015b. A global satellite-assisted precipitation climatology. Earth System Science Data, 7(2): 275-287.

Gao Y.C., Liu M.F., 2013. Evaluation of high-resolution satellite precipitation products using rain gauge observations over the Tibetan Plateau. Hydrology and Earth System Sciences, 17(2): 837-849.

Gao Z., Long D., Tang G., Zeng C., Huang J., Hong Y., 2017. Assessing the potential of satellite-based precipitation estimates for flood frequency analysis in ungauged or poorly gauged tributaries of China's Yangtze River basin. Journal of Hydrology, 550: 478-496.

Guo Z. et al., 2006. Evaluation of the Second Global Soil Wetness Project soil moisture simulations: 2. Sensitivity to external meteorological forcing. Journal of Geophysical Research: Atmospheres (1984–2012).

Han P., Long D., Han Z., Du M., Dai L., Hao X., 2019. Improved understanding of snowmelt runoff from the headwaters of China's Yangtze River using remotely sensed snow products and hydrological modeling. Remote Sensing of Environment, 224: 44-59.

He J., Yang K., 2011. China Meteorological Forcing Dataset. Cold and Arid Regions Science Data Center at Lanzhou.

Huffman G.J., Bolvin D.T., Nelkin E.J., Wolff D.B., Adler R.F., Gu G., Hong Y., Bowman K.P., Stocker E.F., 2007. The TRMM Multisatellite Precipitation Analysis (TMPA): Quasi-Global, Multiyear, Combined-Sensor Precipitation Estimates at Fine Scales. Journal of Hydrometeorology, 8(1): 38-55.

Hwang T., Band L.E., Miniat C.F., Song C., Bolstad P.V., Vose J.M., Love J.P., 2014. Divergent phenological response to hydroclimate variability in forested mountain watersheds. Global Change Biology, 20(8): 2580-2595.

Ji Z., Kang S., 2015. Evaluation of extreme climate events using a regional climate model for China. International Journal of Climatology, 35(6): 888-902.

Jolly W.M., Nemani R., Running S.W., 2005. A generalized, bioclimatic index to predict foliar phenology in response to climate. Global Change Biology, 11(4): 619-632.

Joyce R.J., Janowiak J.E., Arkin P.A., Xie P., 2004. CMORPH: A Method that Produces Global Precipitation Estimates from Passive Microwave and Infrared Data at High Spatial and Temporal Resolution. Journal of Hydrometeorology, 5(3): 487-503.

Kato H., Rodell M., Beyrich F., Cleugh H., van Gorsel E., Liu H., Meyers T.P., 2007. Sensitivity of Land Surface Simulations to Model Physics, Land Characteristics, and Forcings, at Four CEOP Sites. Journal of the Meteorological Society of Japan. Ser. II, 85A: 187-204.

Kavetski D., Kuczera G., Franks S.W., 2006a. Bayesian analysis of input uncertainty in hydrological modeling: 2. Application. Water Resources Research, 42(3).

Kavetski D., Kuczera G., Franks S.W., 2006b. Bayesian analysis of input uncertainty in hydrological modeling: 1. Theory. Water Resources Research, 42(3).

Koch J., Siemann A., Stisen S., Sheffield J., 2016. Spatial validation of large - scale land surface models against monthly land surface temperature patterns using innovative performance metrics. Journal of Geophysical Research: Atmospheres, 121(10): 5430-5452.

Liu W., Wang L., Sun F., Li Z., Wang H., Liu J., Yang T., Zhou J., Qi J., 2018. Snow Hydrology in the Upper Yellow River Basin Under Climate Change: A Land Surface Modeling Perspective. Journal of Geophysical Research: Atmospheres, 123(22).

Matthew R., Hiroko Kato B., 2015. GLDAS Noah Land Surface Model L4 3 hourly 0.25 x 0.25 degree V2.0. NASA/GSFC/HSL, Goddard Earth Sciences Data and Information Services Center (GES DISC), Greenbelt, Maryland, USA.

Matthew R., Hiroko Kato B., 2016. GLDAS Noah Land Surface Model L4 3 hourly 0.25 x 0.25 degree V2.1. NASA/GSFC/HSL, Goddard Earth Sciences Data and Information Services Center (GES DISC), Greenbelt, Maryland, USA.

Park C.-E. et al., 2018. Keeping global warming within 1.5 °C constrains emergence of aridification. Nature Climate Change, 8(1): 70-74.

Qi W., Zhang C., Fu G., Zhou H., 2015. Global Land Data Assimilation System data assessment using a distributed biosphere hydrological model. Journal of Hydrology, 528: 652-667.

Qi W., Zhang C., Fu G., Sweetapple C., Zhou H., 2016a. Evaluation of global fine-resolution precipitation products and their uncertainty quantification in ensemble discharge simulations. Hydrology and Earth System Sciences, 20(2): 903-920.

Qi W., Zhang C., Fu G., Zhou H., 2016b. Quantifying dynamic sensitivity of optimization algorithm parameters to improve hydrological model calibration. Journal of Hydrology, 533: 213-223.

Qi W., Zhang C., Fu G., Zhou H., Liu J., 2016c. Quantifying uncertainties in extreme flood predictions under climate change for a medium-sized basin in northeast China. Journal of Hydrometeorology(17): 3099–3112.

Qi W., Liu J., Chen D., 2018a. Evaluations and Improvements of GLDAS2.0 and GLDAS2.1 Forcing Data's Applicability for Basin Scale Hydrological Simulations in the Tibetan Plateau. Journal of Geophysical Research: Atmospheres, 123.

Qi W., Liu J., Yang H., Sweetapple C., 2018b. An ensemble-based dynamic Bayesian averaging approach for discharge simulations using multiple global precipitation products and hydrological models. Journal of Hydrology, 558.

Qi W., Zhang C., Fu G., Sweetapple C., Liu Y., 2018c. Impact of robustness of hydrological model parameters on flood prediction uncertainty. Journal of Flood Risk Management, e12488.

Qi W., Liu J., Leung F., 2019. A framework to quantify impacts of elevated CO2 concentration, global warming and leaf area changes on seasonal variations of water resources on a river basin scale. Journal of Hydrology, 570: 508-522.

Rodell M. et al., 2004. The Global Land Data Assimilation System. Bulletin of the American Meteorological Society, 85(3): 381-394.

Schellekens J. et al., 2017. A global water resources ensemble of hydrological models: the eartH2Observe Tier-1 dataset. Earth System Science Data, 9(2): 389-413.

Sellers P.J., Mintz Y., Sud Y.C., Dalcher A., 1986. A Simple Biosphere Model (SIB) for Use within General Circulation Models. Journal of the Atmospheric Sciences, 43(6): 505-531.

Sellers P.J., Randall D.A., Collatz G.J., Berry J.A., Field C.B., Dazlich D.A., Zhang C., Collelo G.D., Bounoua L., 1996a. A Revised Land Surface Parameterization (SiB2) for Atmospheric GCMS. Part I: Model Formulation. Journal of Climate, 9(4): 676-705.

Sellers P.J., Tucker C.J., Collatz G.J., Los S.O., Justice C.O., Dazlich D.A., Randall D.A., 1996b. A Revised Land Surface Parameterization (SiB2) for Atmospheric GCMS. Part II: The Generation of Global Fields of Terrestrial Biophysical Parameters from Satellite Data. Journal of Climate, 9(4): 706-737.

Shen Y., Xiong A., 2016. Validation and comparison of a new gauge - based precipitation analysis over mainland China. International Journal of Climatology, 36(1): 252-265.

Silvestro F., Gabellani S., Rudari R., Delogu F., Laiolo P., Boni G., 2015. Uncertainty reduction and parameter estimation of a distributed hydrological model with ground and remote-sensing data. Hydrology and Earth System Sciences, 19(4): 1727-1751.

Sobol I.M., 2001. Global sensitivity indices for nonlinear mathematical models and their Monte Carlo estimates. Mathematics and Computers in Simulation, 55(1-3).

Tang Y., Reed P., van Werkhoven K., Wagener T., 2007a. Advancing the identification and evaluation of distributed rainfall - runoff models using global sensitivity analysis. Water Resources Research, 43(6).

Tang Y., Reed P., Wagener T., Werkhoven K.v., 2007b. Comparing sensitivity analysis methods to advance lumped watershed model identification and evaluation. Hydrology and Earth System Sciences, 11.

van der Ent R.J., Wang-Erlandsson L., Keys P.W., Savenije H.H.G., 2014. Contrasting roles of interception and transpiration in the hydrological cycle – Part 2: Moisture recycling. Earth System Dynamics, 5(2): 471-489.

Vano J.A., Das T., Lettenmaier D.P., 2012. Hydrologic Sensitivities of Colorado River Runoff to Changes in Precipitation and Temperature. Journal of Hydrometeorology, 13: 932-949.

Wan Z., 2008. New refinements and validation of the MODIS Land-Surface Temperature/Emissivity products. Remote Sensing of Environment, 112(1): 59-74.

Wang-Erlandsson L., van der Ent R.J., Gordon L.J., Savenije H.H.G., 2014. Contrasting roles of interception and transpiration in the hydrological cycle – Part 1: Temporal characteristics over land. Earth System Dynamics, 5(2): 441-469.

Wang A., Zeng X., 2011. Sensitivities of terrestrial water cycle simulations to the variations of precipitation and air temperature in China. Journal of Geophysical Research: Atmospheres (1984–2012), 116(D2).

Wang F., Wang L., Koike T., Zhou H., Yang K., Wang A., Li W., 2011. Evaluation and application of a fine-resolution global data set in a semiarid mesoscale river basin with a distributed biosphere hydrological model. Journal of Geophysical Research: Atmospheres, 116(D21).

Wang F., Wang L., Zhou H., Saavedra Valeriano O.C., Koike T., Li W., 2012. Ensemble hydrological prediction-based real-time optimization of a multiobjective reservoir during flood season in a semiarid basin with global numerical weather predictions. Water Resources Research, 48(7).

Wang L., Koike T., Yang D.W., Yang K., 2009a. Improving the hydrology of the Simple Biosphere Model 2 and its evaluation within the framework of a distributed hydrological model. Hydrological Sciences Journal, 54(6): 989-1006.

Wang L., Koike T., Yang K., Jackson T.J., Bindlish R., Yang D., 2009b. Development of a distributed biosphere hydrological model and its evaluation with the Southern Great Plains Experiments (SGP97 and SGP99). Journal of Geophysical Research: Atmospheres, 114(D8).

Wang L., Koike T., Yang K., Yeh P.J.-F., 2009c. Assessment of a distributed biosphere hydrological model against streamflow and MODIS land surface temperature in the upper Tone River Basin. Journal of Hydrology, 377(1-2): 21-34.

Wang L., Koike T., Yang K., Jin R., Li H., 2010a. Frozen soil parameterization in a distributed biosphere hydrological model. Hydrology and Earth System Sciences, 14(3): 557-571.

Wang L., Wang Z., Koike T., Yin H., Yang D., He S., 2010b. The assessment of surface water resources for the semi-arid Yongding River Basin from 1956 to 2000 and the impact of land use change. Hydrological Processes, 24(9): 1123-1132.

Wang L., Sun L., Shrestha M., Li X., Liu W., Zhou J., Yang K., Lu H., Chen D., 2016. Improving snow process modeling with satellite‐based estimation of near‐surface‐air‐temperature lapse rate. Journal of Geophysical Research: Atmospheres, 121(20).

Weedon G.P., Balsamo G., Bellouin N., Gomes S., Best M.J., Viterbo P., 2014. The WFDEI meteorological forcing data set: WATCH Forcing Data methodology applied to ERA‐Interim reanalysis data. Water Resources Research, 50(9): 7505-7514.

Wei J., Dirmeyer P.A., Guo Z., 2008. Sensitivities of soil wetness simulation to uncertainties in precipitation and radiation. Geophysical Research Letters, 35(15).

Weiland F.C., Vrugt J.A., Weerts A.H., Bierkens M.F.P., 2015. Significant uncertainty in global scale hydrological modeling from precipitation data errors. Journal of Hydrology, 529: 1095-1115.

Xue B.L. et al., 2013. Modeling the land surface water and energy cycles of a mesoscale watershed in the central Tibetan Plateau during summer with a distributed hydrological model. Journal of Geophysical Research: Atmospheres, 118(16): 8857-8868.

Yang D., 1998. Distributed hydrological model using hillslope discretization based on catchment area function: development and applications, University of Tokyo, Tokyo.

Yang F., Lu H., Yang K., He J., Wang W., Wright J.S., Li C., Han M., Li Y., 2017. Evaluation of multiple forcing data sets for precipitation and shortwave radiation over major land areas of China. Hydrology and Earth System Sciences, 21(11): 5805-5821.

Yang K., Wu H., Qin J., Lin C., Tang W., Chen Y., 2014. Recent climate changes over the Tibetan Plateau and their impacts on energy and water cycle: A review. Global and Planetary Change, 112: 79-91.

Zhang C., Chu J., Fu G., 2013a. Sobol′’s sensitivity analysis for a distributed hydrological model of Yichun River Basin, China. Journal of Hydrology, 480: 58-68.

Zhang L., Su F., Yang D., Hao Z., Tong K., 2013b. Discharge regime and simulation for the upstream of major rivers over Tibetan Plateau. Journal of Geophysical Research: Atmospheres, 118(15): 8500-8518.

Zhao Y., Zhu J., 2015. Assessing Quality of Grid Daily Precipitation Datasets in China in Recent 50 Years (in Chinese). PLATEAU METEOROLOGY, 34(1): 50-58.

Zhou J., Wang L., Zhang Y., Guo Y., Li X., Liu W., 2015. Exploring the water storage changes in the largest lake (Selin Co) over the Tibetan Plateau during 2003–2012 from a basin‐wide hydrological modeling. Water Resources Research, 51(10): 8060-8086.

Zhou X.Y., Zhang Y.Q., Yang Y.H., Yang Y.M., Han S.M., 2013. Evaluation of anomalies in GLDAS-1996 dataset. Water Science and Technology, 67(8): 1718-1727.

Table 1 Average LAI, aridity index, climate and hydrological regimes based on data from 2000 to 2010 in the river basins studied

River basin	Average LAI	Average aridity index (P/PET), climate and hydrological regimes
Yarlung Tsangpo River	0.22	1.09, Humid, Energy-limited
Upper Yellow River	0.55	0.63, Dry sub-humid, Water-limited
Upper Lancang River	0.43	0.42, Semi-arid, Water-limited
Upper Yangtze River	0.23	0.41, Semi-arid, Water-limited

Note. LAI = Leaf Area Index; P = Precipitation; PET = Potential Evaporation Transpiration; Humid zone = Aridity Index > 0.65; Sub-humid zone = 0.5 < Aridity Index < 0.65; Semiarid zone = 0.2 < Aridity Index < 0.5. Climate zones are defined based on the study by Park et al. (2018); PET is calculated using the Penman-Monteith method; MODIS MOD15A2 LAI product is used to calculate the average LAI.

Table 2 The global precipitation products used

Product	Spatial resolution	Temporal resolution	Reference
TRMM3B42 V7	0.25°	3h	Huffman et al. (2007)
CMORPH-BLD 1.0	0.25°	Daily	Joyce et al. (2004)
CHIRPS V2.0	0.25°	Daily	Funk et al. (2015a); Funk et al. (2015b)
MSWEP V2.01	0.25°	3h	Beck et al. (2017)
WFDEI-CRU	0.5°	3h	Weedon et al. (2014)
PERSIANN-CDR	0.25°	Daily	Ashouri et al. (2015)
GLDAS2.0	0.25°	3h	Matthew and Hiroko Kato (2015)
GLDAS2.1	0.25°	3h	Matthew and Hiroko Kato (2016)

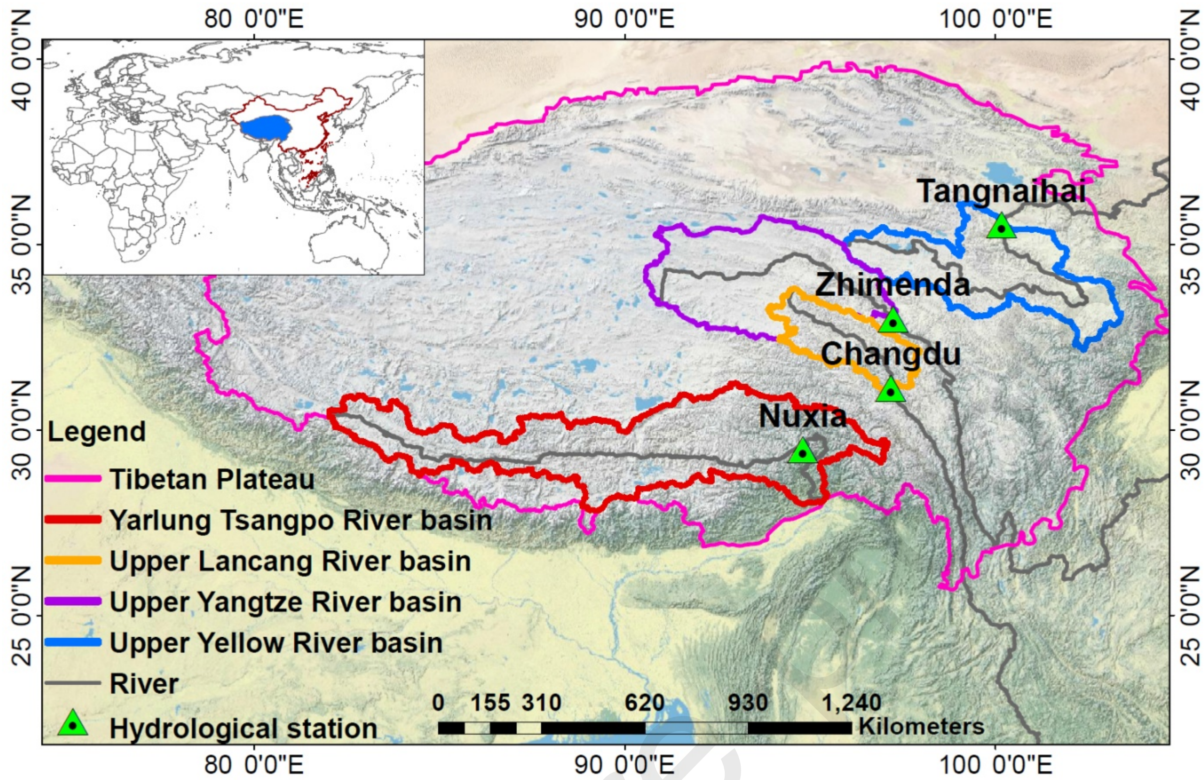

Fig. 1 The river basins studied in the Tibetan Plateau.

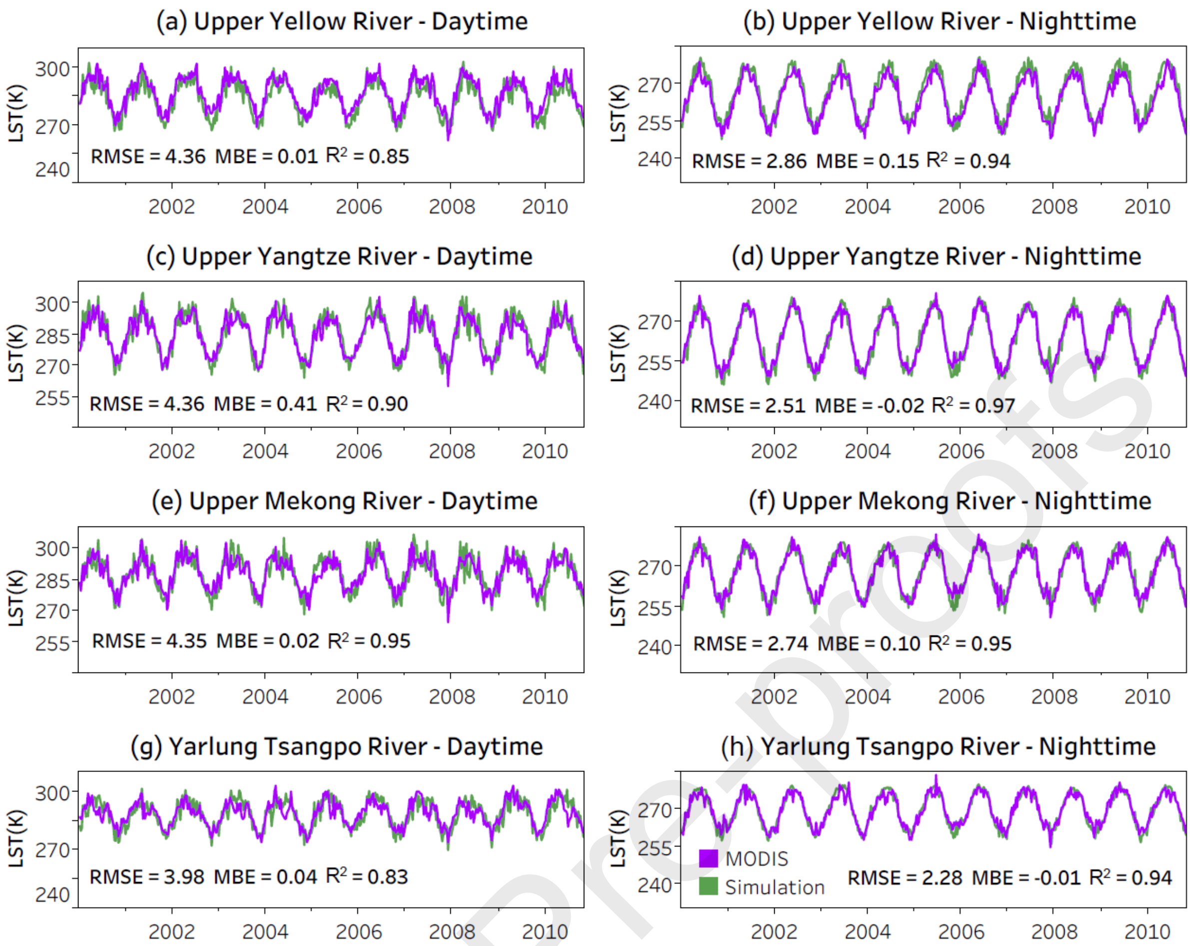

Fig. 2 8-day land surface temperature (LST) comparison between MODIS observation and WEB-DHM simulation in the four large river basins in the Tibetan Plateau. RMSE = root mean square error; MBE = mean bias error.

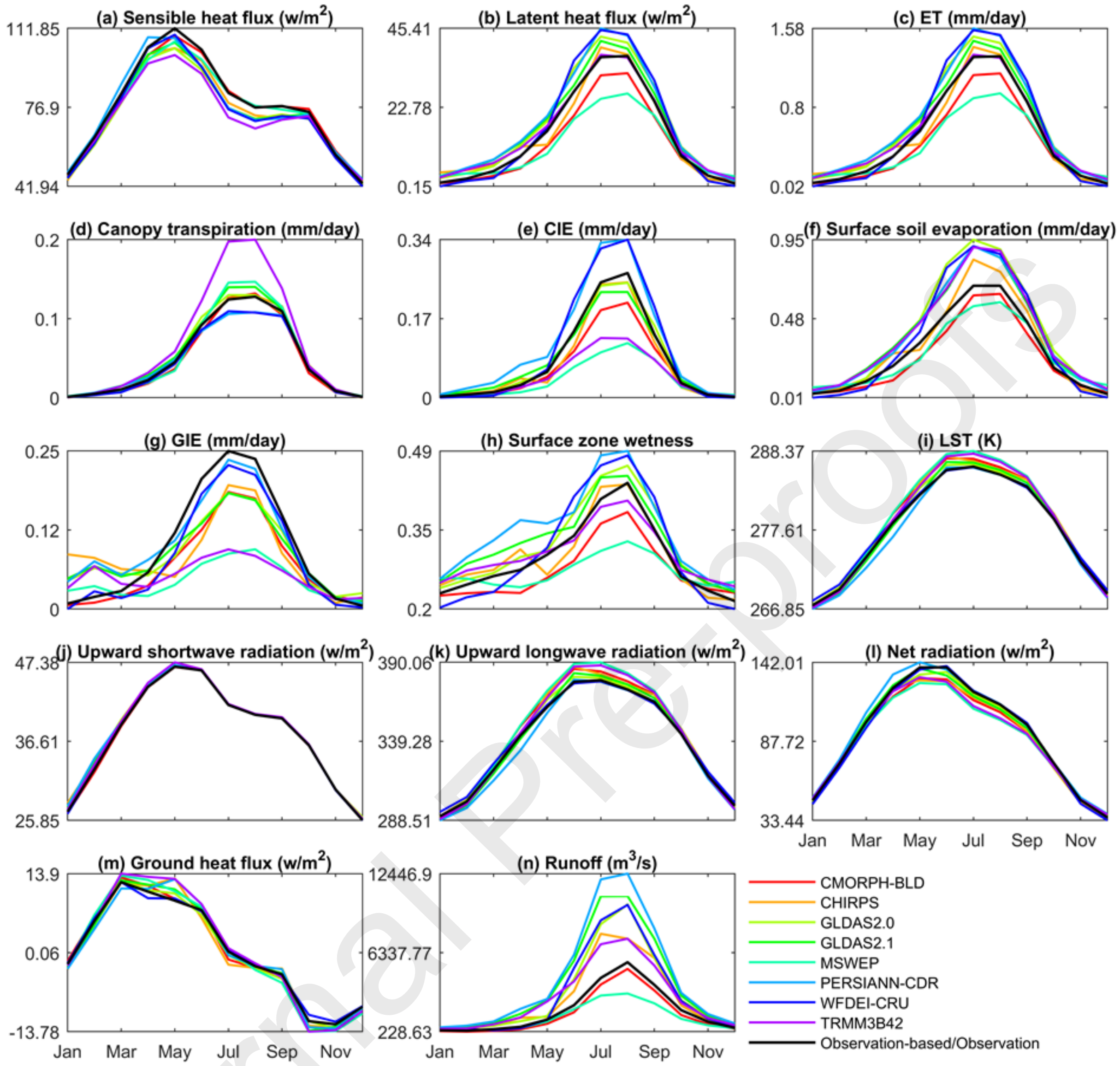

Fig. 3 Ensemble of long term mean monthly simulation results in the Yarlong Tsangpo River basin using different global precipitation products. ET = Evapotranspiration; CIE = Canopy interception loss; GIE = Ground interception store evaporation; LST = Land surface temperature. For runoff and LST, the plotted data are observation. 'Observation-based' refers to simulation using observation.

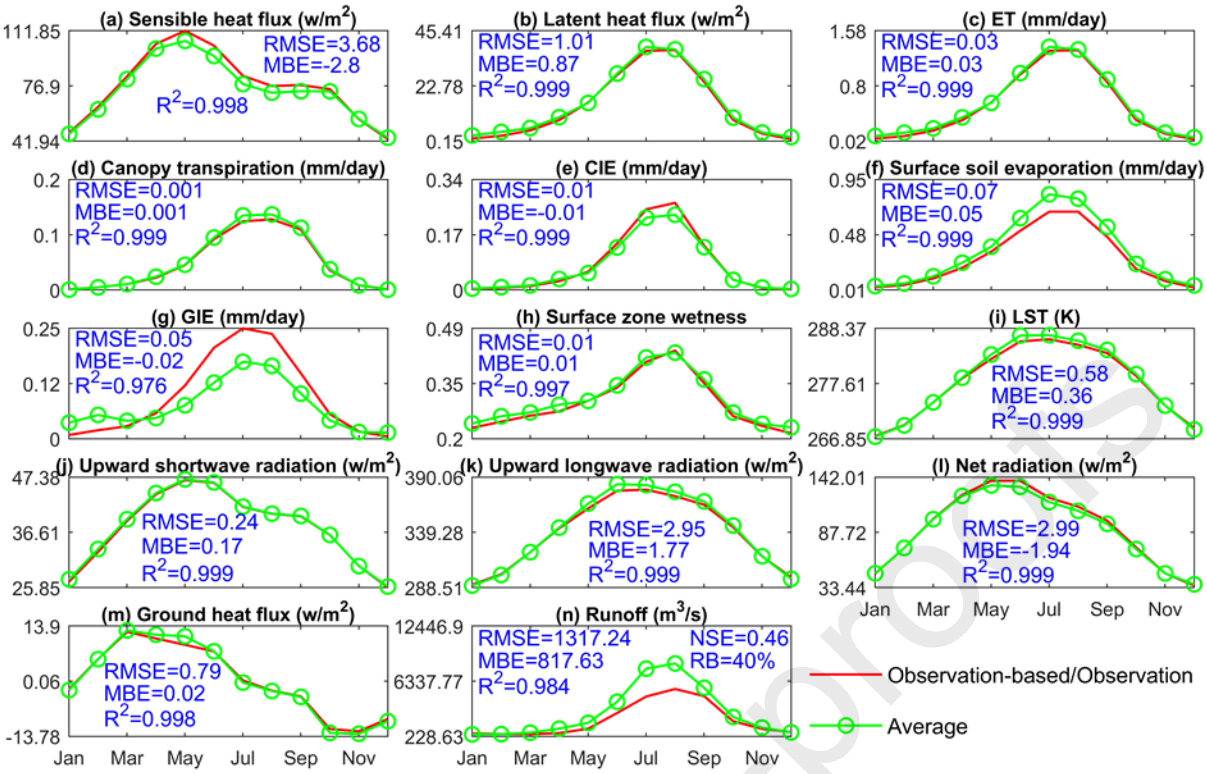

Fig. 4 Comparison between ensemble averages and observation/observation-based simulation results in the Yarlong Tsangpo River basin. ET = Evapotranspiration; CIE = Canopy interception loss; GIE = Ground interception store evaporation; LST = Land surface temperature. For runoff and LST, the plotted data are observation. 'Observation-based' refers to simulation using observation.

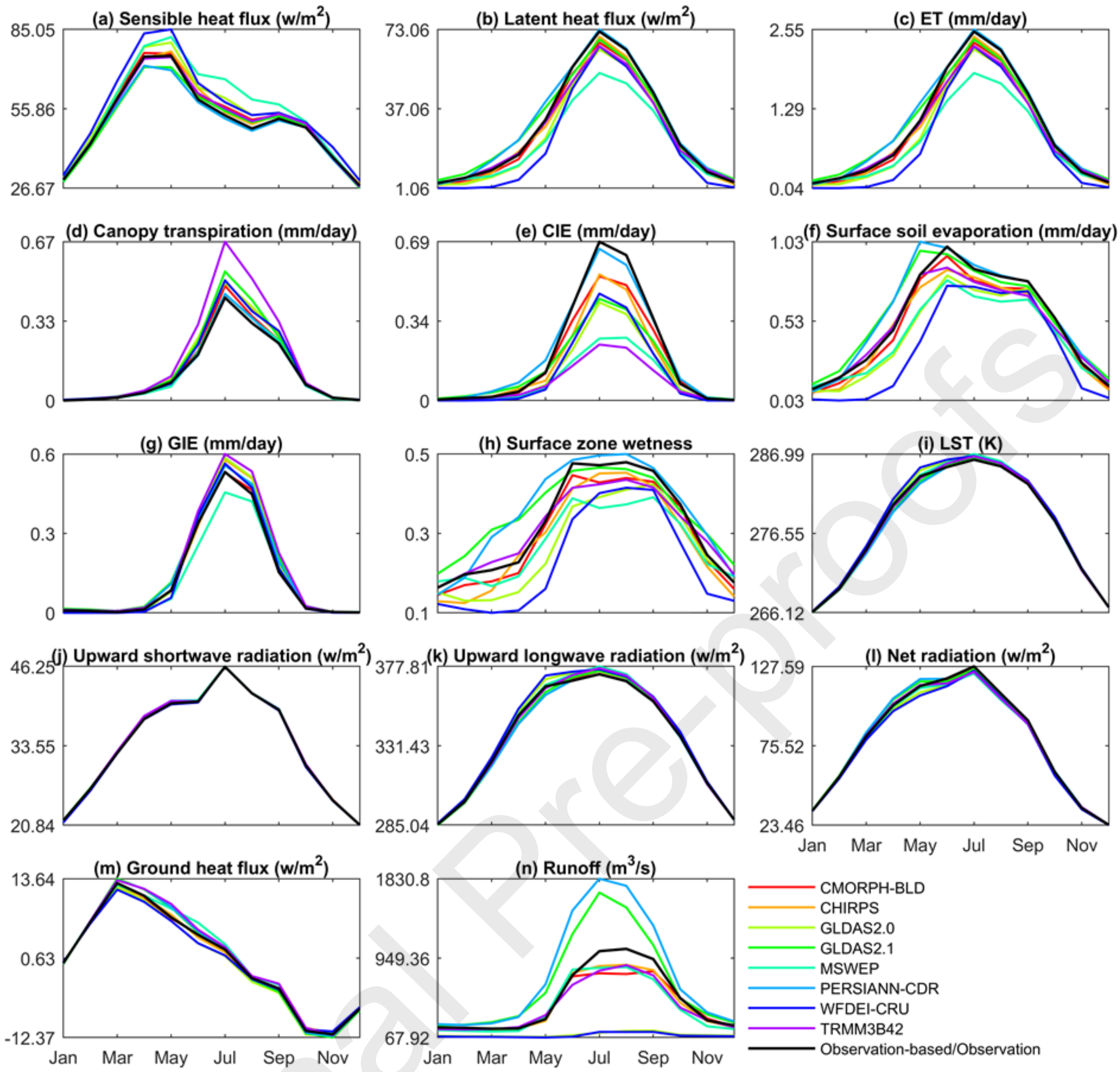

Fig. 5 Long term mean monthly simulation results in the Upper Lancang River basin using different global precipitation products. ET = Evapotranspiration; CIE = Canopy interception loss; GIE = Ground interception store evaporation; LST = Land surface temperature. For runoff and LST, the plotted data are observation. 'Observation-based' refers to simulation using observation.

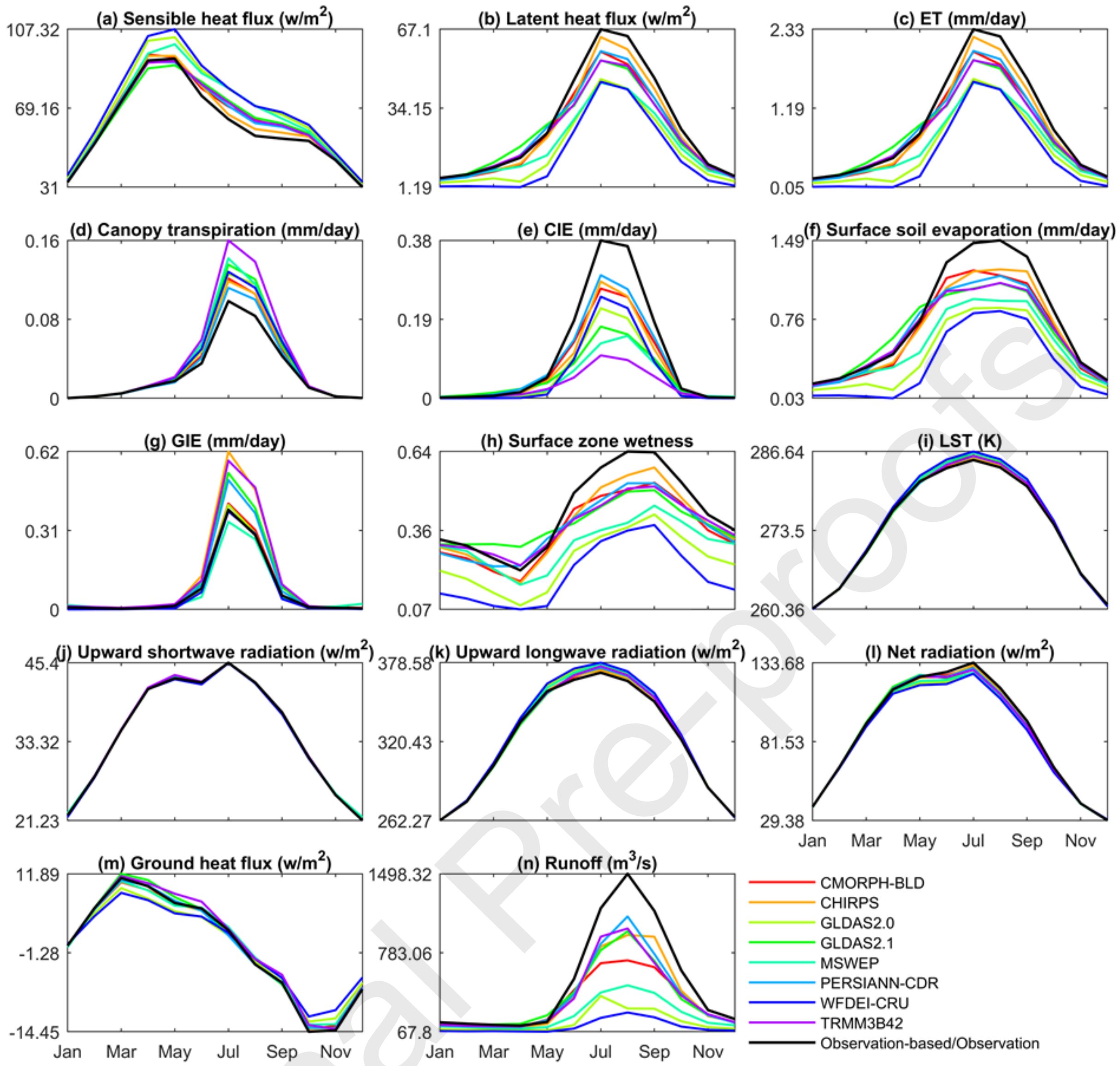

Fig. 6 Long term mean monthly simulation results in the Upper Yangtze River basin using different global precipitation products. ET = Evapotranspiration; CIE = Canopy interception loss; GIE = Ground interception store evaporation; LST = Land surface temperature. For runoff and LST, the plotted data are observation. ‘Observation-based’ refers to simulation using observation.

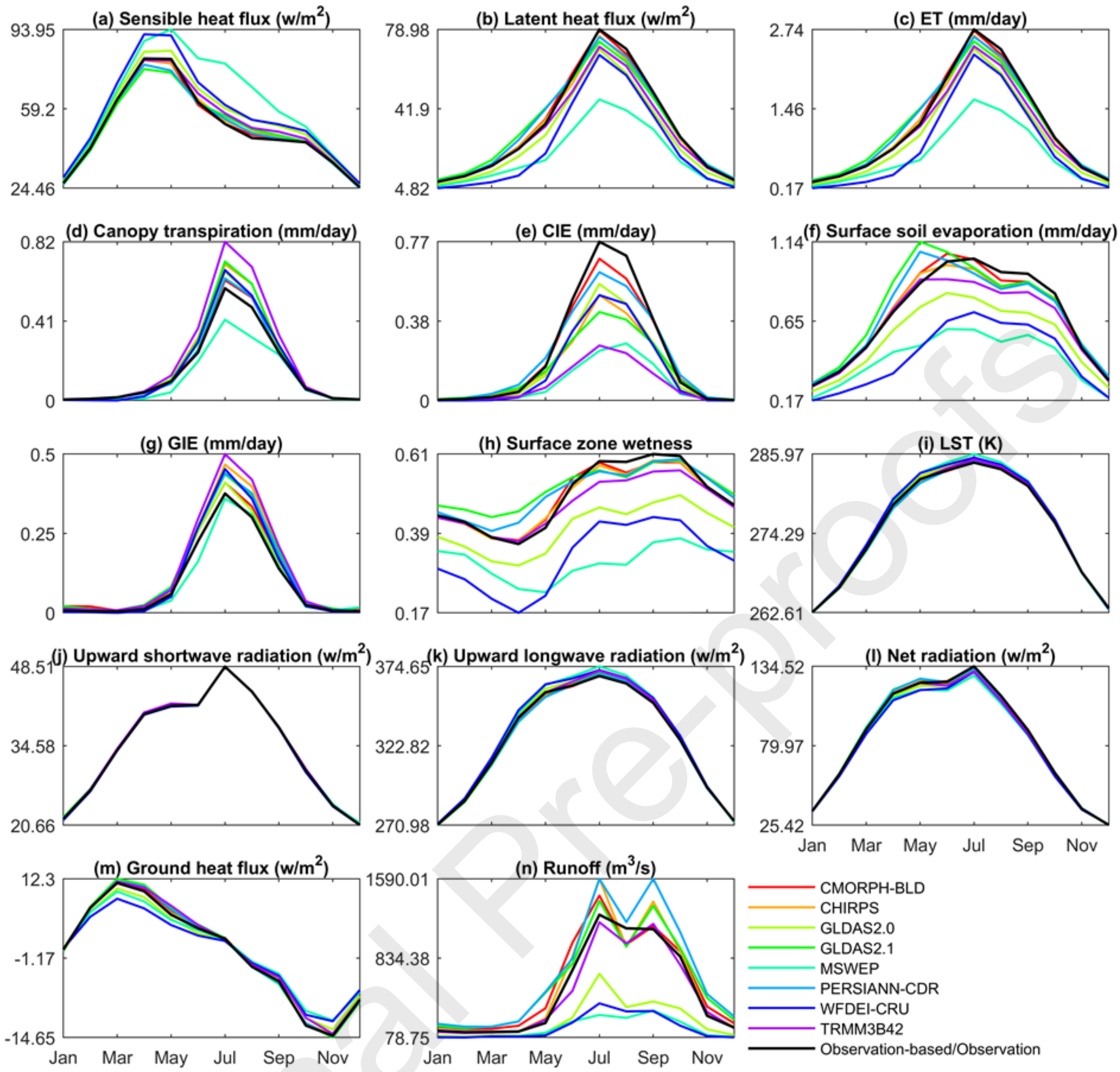

Fig. 7 Long term mean monthly simulation results in the Upper Yellow River basin using different global precipitation products. ET = Evapotranspiration; CIE = Canopy interception loss; GIE = Ground interception store evaporation; LST = Land surface temperature. For runoff and LST, the plotted data are observation. ‘Observation-based’ refers to simulation using observation.

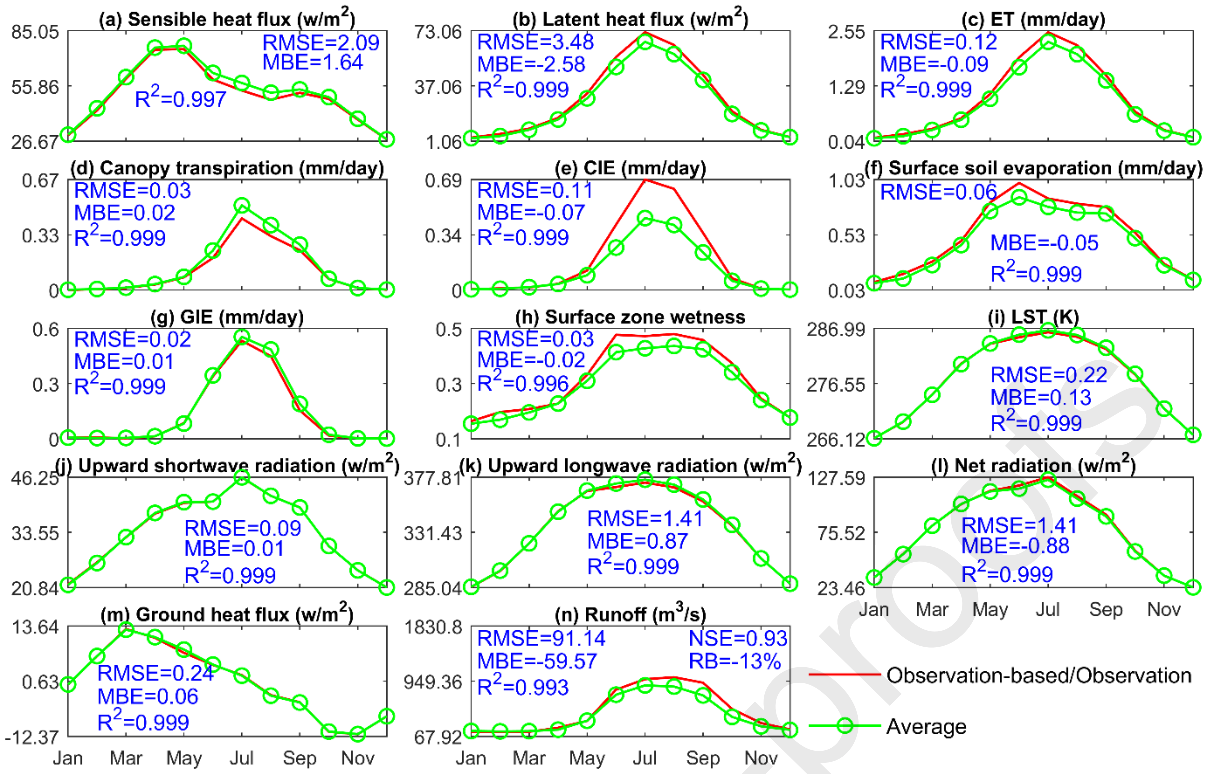

Fig. 8 Comparison between ensemble averages and observation/observation-based simulation results in the Upper Lancang River basin. ET = Evapotranspiration; CIE = Canopy interception loss; GIE = Ground interception store evaporation; LST = Land surface temperature. For runoff and LST, the plotted data are observation. 'Observation-based' refers to simulation using observation.

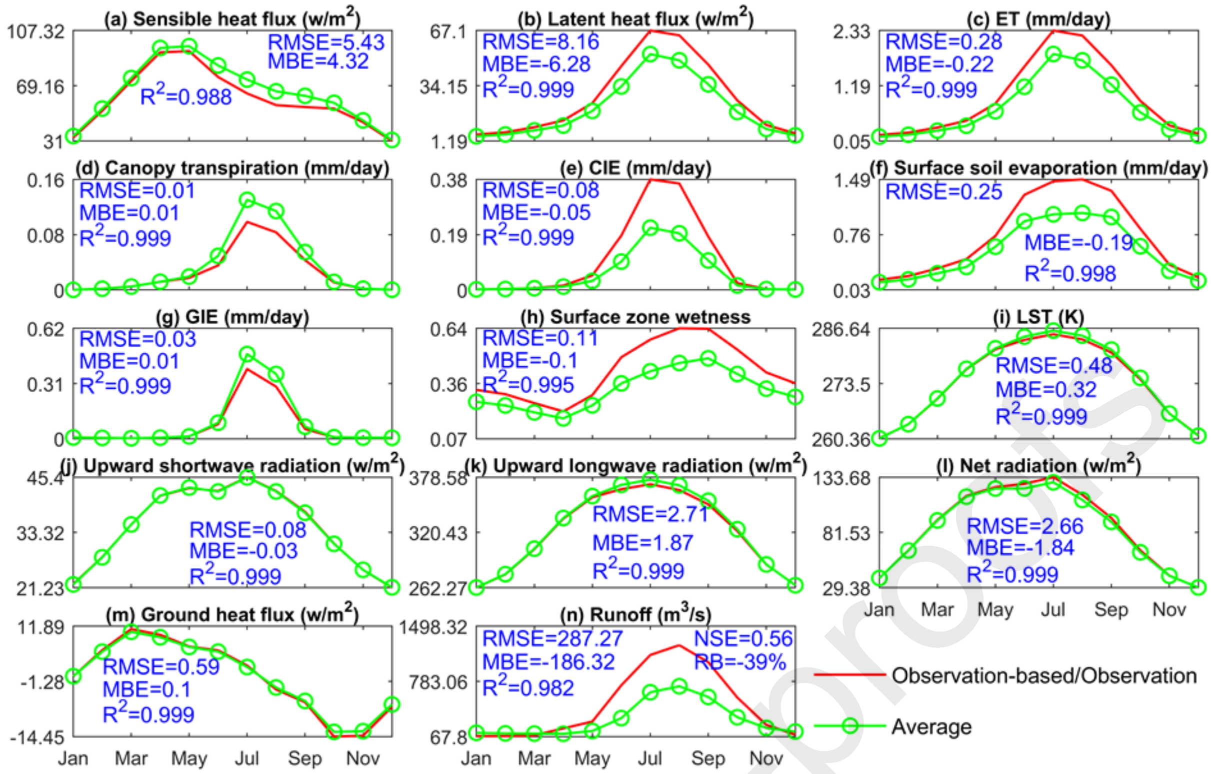

Fig. 9 Comparison between ensemble averages and observation/observation-based simulation results in the Upper Yangtze River basin. ET = Evapotranspiration; CIE = Canopy interception loss; GIE = Ground interception store evaporation; LST = Land surface temperature. For runoff and LST, the plotted data are observation. ‘Observation-based’ refers to simulation using observation.

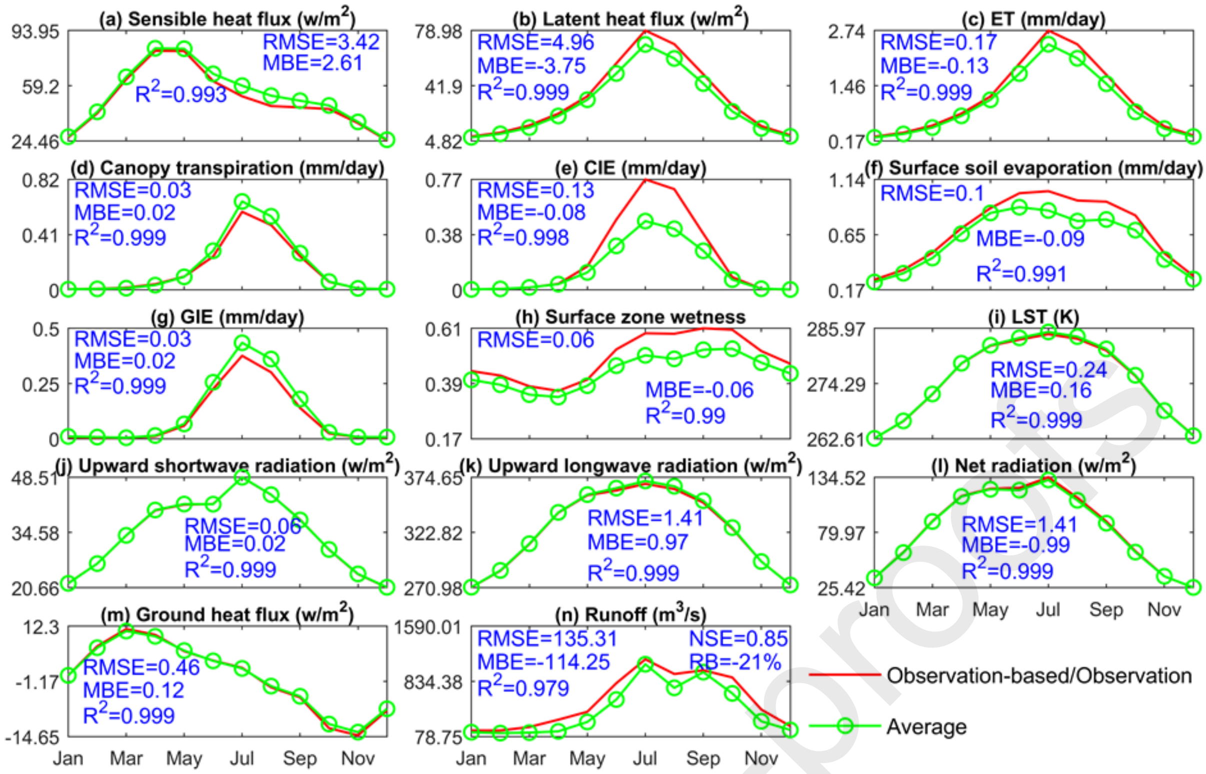

Fig. 10 Comparison between ensemble averages and observation/observation-based simulation results in the Upper Yellow River basin. ET = Evapotranspiration; CIE = Canopy interception loss; GIE = Ground interception store evaporation; LST = Land surface temperature. For runoff and LST, the plotted data are observation. 'Observation-based' refers to simulation using observation.

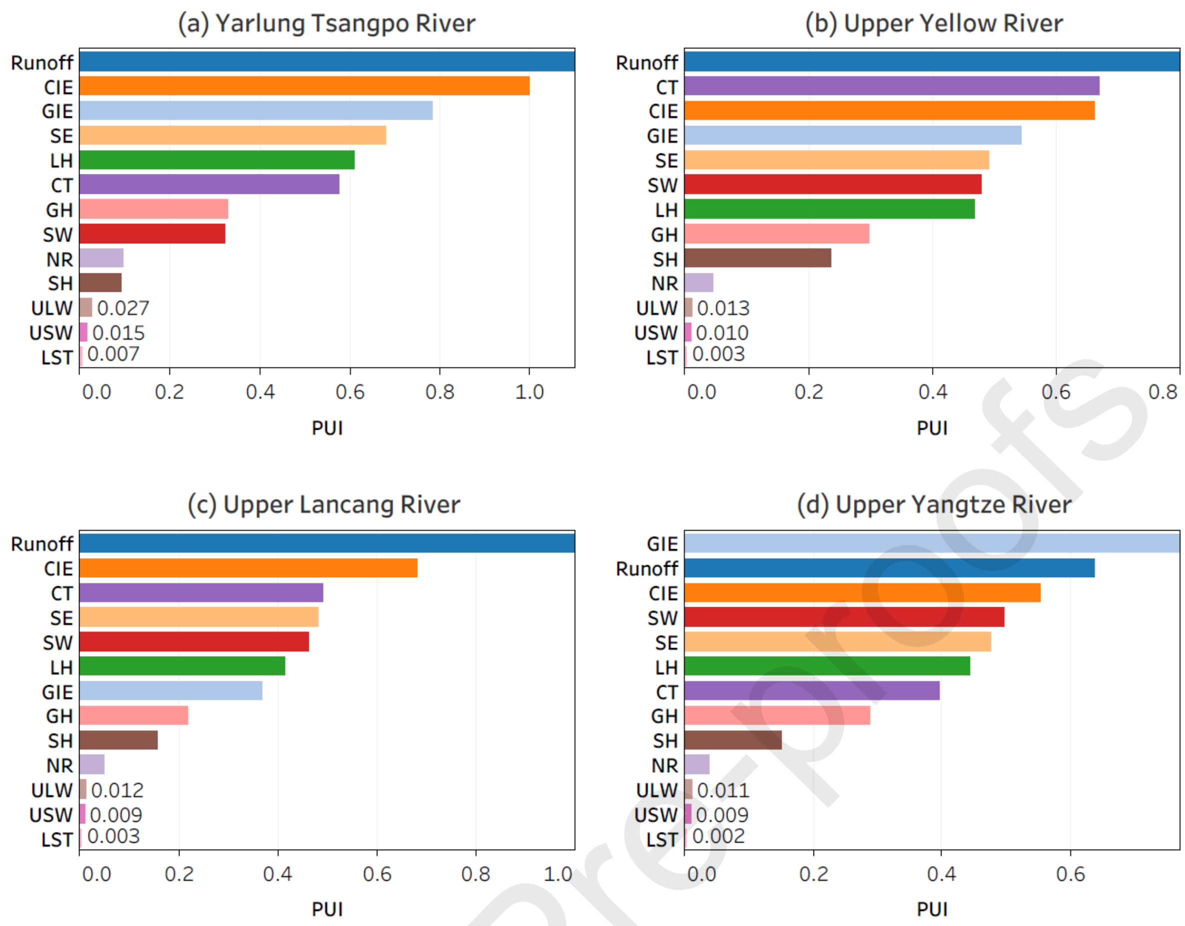

Fig. 11 Precipitation Uncertainty Influence (PUI) on water and energy variables. The higher the PUI values, the greater the influence. CIE = Canopy interception loss; GIE = Ground interception store evaporation; SE = Surface soil evaporation; LH = Latent heat flux; CT = Canopy transpiration; GH = Ground heat flux; SH = Sensible heat flux; SW = Surface zone wetness; NR = Net radiation; ULW = Upward longwave radiation; USW = Upward shortwave radiation; LST = Land surface temperature.

Highlights:

Develop an approach to quantify sensitivity of land surface simulation to rainfall

Intercompare sensitivity of surface water and energy variables in the Tibetan Plateau

Canopy interception loss and runoff are sensitive to rainfall uncertainty

Land surface temperature is not sensitive to rainfall uncertainty